ISSN: 0067-2904

Noble Metals/NiO Core- Shell Based Gas Sensors

Iftikhar M. Ali*
Department of Physics, College of Science, University of Baghdad, Baghdad, Iraq

Abstract:

The application of novel core-shell nanostructure composed of Cu, Ag, Au/NiO to improve the sensitivity of pure NiO to H_2S gas sensors is demonstrated in this study. The growth of Cu, Ag, Au/NiO core-shell nanostructure is performed by chemical reaction of NiO on metal nanoparticle (Cu, Ag and Au) that prepared by pulsed laser ablation (PLA) technique. This is to form the homogeneous structure of the sensors investigated in this report to assess their sensitivity in terms of H_2S detection. These novel H_2S gas sensors were evaluated at operating temperatures of 25 °C, 100 °C and at 150 °C. The result reveals the Cu, Ag, Au/NiO core-shell nanostructure present a good sensitivity at low working temperatures compared by pure NiO nanoparticles. These core-shell nanostructure sensors also possess the highest response (<32 s) and recovery (<28 s) values with greater repeatability seen for H_2S sensors at low temperatures, unlike traditional sensors that only work effectively at much higher temperatures. The data in this study indicates the newly-developed Cu, Ag, Au/NiO core-shell nanostructure based sensors are highly promising for industrial applications.

Keywords: NiO, Cu/NiO, Ag/NiO, Au/NiO; core shell; nanostructure; H_2S; gas sensor; sensitivity.

المعادن النبيلة / اوكسيد النيكل لب– قشرة كمتحسسات غازية

افتخار محمود علي*
قسم الفيزياء، كلية العلوم، جامعة بغداد، بغداد، العراق

الخلاصة

التطبيق المبتكر للتركيب النانوي لب–قشرة المتكون من نحاس، فضة، ذهب / اوكسيد النيكل لتحسين تحسسية اوكسيد النيكل النقي قد تم إظهاره في هذه الدراسة. ان انماء التركيب النانوي لب–قشرة من نحاس، فضة، ذهب / اوكسيد النيكل يرسب بالتفاعل الكيميائي لأوكسيد النيكل مع جسيمات معدن النحاس، الفضة، الذهب النانوية المحضرة بتقنية الاجتثاث بالليزر النبضي لتكوين تركيب متجانس للمتحسسات لتقييم تحسسيتها في الكشف عن غاز كبريتيد الهيدروجين عند درجات حرارة 25، 100، 150 ^{o}م. وضحت النتائج بان التركيب النانوي لب–قشرة من نحاس، فضة، ذهب / اوكسيد النيكل له تحسسية جيدة عند درجات تشغيل واطئة مقارنة بأوكسيد النيكل النقي. ان المتحسسات ذات التركيب النانوي لب–قشرة تمتلك قيم استجابة سريعة بزمن استجابة سريع اقل من 32 ثانية وبزمن نزول اقل من 28 ثانية وبتكرارية جيدة لمتحسسات كبريتيد الهيدروجين عند درجات حرارية منخفضة مقارنة بالمتحسسات التقليدية التي تعمل بفعالية عالية فقط عند درجات حرارية عالية جداً. في هذه الدراسة تشير القيم الى امكانية تصنيع متحسسات جديدة ومطورة مبنية من التركيب النانوي لب–قشرة من نحاس، فضة، ذهب / اوكسيد النيكل لتطبيقات صناعية واعدة.

*Email: iftikhariq@gmail.com

1. Introduction

Due to an increase in atmospheric pollution, there is a need to fabricate sensitive devices to detect and measure different hazardous gases. Currently, standard air pollution measurements are based on expensive optical spectroscopy and gas chromatography techniques. These techniques are large, expensive and slow in terms of reaction times [1, 2]. Therefore, there is an urgent need to design and fabricate cheap gas sensor devices to detect diverse explosive and toxic gases.

Over the past decades, metal oxide semiconductors are interested to be used in gas sensors field. Various types of metal oxide based sensors composed of TiO2, SnO2, ZnO, or WO3 have been used extensively to detect toxic and pollutant gases, such as NOx, H2S, Cl2, CO, SO2, and O3. Other combustible gases, including H2, CH4 and flammable organic vapors are also detectable by these compound based sensors [3-5].

Metal oxide thin films are fabricated by dry/wet techniques. The microstructure of fabricated thin film is closely associated to the fabrication process. By altering deposition parameters, the microstructure changes and the gas sensing performance of film changes respectively. Grain size and porosity are two important parameters for metal oxide gas sensors [6,7]. Among the metal oxide semiconductors, nickel oxide has drawn significant interest owing to its wide range of applications. NiO is insulator in a stoichiometric ratio, and its non-stoichiometry semiconducting behavior attributed to the percentage of Ni^{+2} vacancies in NiO of the prepared sample [8]. There are few studies on the gas sensing property of NiO. Nickel oxide is chemically and thermally stable p-type semiconductor can be used in optical, electronic, catalytic and super-paramagnetic devices like transparent conductor films, gas sensors, alkaline battery cathodes, dye-sensitized solar cells and solid oxide fuel cells (SOFC)[9-16]. It is also noted that the use of semiconductor metal oxide materials for gas sensing generally involves some chemical reaction with gas molecules on the oxide surface [17].

Hydrogen sulfide (H_2S) is a colorless gas with the characteristic foul odor of rotten eggs; it is heavier than air, very poisonous, corrosive, flammable, and explosive. An ideal sensor can be utilized in an early warning system for environmental monitoring to detect the presence of H_2S before a critical condition occurs. The demand to produce ideal H_2S sensors has propelled considerable research activities in the relevant fields. It was well known that the sensor characteristics can be changed by varying the crystal structure, dopants, preparation technology, operation temperature, etc[18,19]. Nowadays, also noble metals such as Au, Ag, Pt, Cu and Pd are used as active catalysts. These noble metals enhance the reaction between target gas (especially reduced gases) and oxygen molecules [20]. Production of core–shell nanostructures is an attractive field to improve some properties such as sensing behavior [21,22]. The structure of noble metal/NiO core-shell nanostructures uniquely consists of a noble metal core (Ag, Au, Cu) and NiO shell. Its use in gas sensors has not been formally reported, despite its advantageous characteristics. It is proposed in this study to apply noble metal/NiO core-shell as a novel sensor for H_2S detection. This research reports the manufacturing procedures and its chemical sensing properties for H_2S tracing. The addition of noble metals is also discussed.

2. Experimental Procedure

2.1. Materials and Methods

A) Preparation of Ag, Au, Cu nanoparticles

Formation of Ag, Au, Cu Nanoparticles Silver, gold and copper NPs was fabricated using PLA in distilled water, the metal target (silver, gold and cupper) with purity (99.98%) was immersed in liquid media at room temperature. The volume of liquid is 5 ml. The container placed on the table. The target was irradiated by using a Q-switched Nd:YAG laser beam which operate at (1064) nm wavelength and 10 ns pulse duration. The color of the colloidal suspensions is yellow, red, green for silver, gold, copper respectively, indicates of nanoparticles production. Colloidal solution containing NPs is obtained.

B) Preparation of Nickel Oxide nanoparticles

The chemicals used in this study nickel chloride ($NiCl_2$) and sodium hydroxide (NaOH) as source materials. Chemical precipitation synthesis of NiO nano-powder comprised the following stages: (a) formation of $NiCl_2$ precursor by dissolving 0.1 M $NiCl_2$ in 100ml distilled water, and stirring on magnetic stirrer for 30 min (b) dissolving 1M from NaOH in 50 ml distilled water (c) addition NaOH by drop-wise to 0.1M $NiCl_2$ while vigorous stirring of the solution continued until the pH reached 11 (d) the product is filtered and washed several times with distilled water and finally with acetone to

eliminate the residual byproducts (e) the precipitation was dried in oven at 150 ^{o}C for 5 hr (f) dried green powder will be obtained .

C) core-shell preparation

Ag, Au and Cu nanoparticles have pre-prepared by pulse laser ablation technique separately. The amount is 10ml from these noble metals nanoparticles, stirred on magnetic stirrer. Then repeating the same procedures as in (B). Then the powders are characterized by XRD technique.

2.2. Preparation of substrates

A) Silicon wafer cleaning

n-type (111) oriented Si wafers were used as the substrates. They were initially cleaned by Radio Corporation of America (RCA) standard clean process to remove organic contaminants, and then rinsed under running distilled water. To thoroughly remove native oxide, the wafers were dipped into 48% HF solution for 10 seconds, and flushed by dry air. Then they will be ready to use.

B) Glass slide cleaning

Glass slide were cleaned by ethanol then in distilled water for 15 min in ultrasonic bath then dried in oven at 50^{o}C for 1 hr.

2.3. Sample preparation

(25mg) nano powders was dispersed in ethanol and dropped on the substrates to prepare thin films by spin coating technique and dry in oven at 100^{o}C for 2 min. This step is repeated for 10 times to obtain the final thickness (100±10) nm.

2.4. Characterization techniques

In order to study the structural properties for prepared powders, the crystalline structure was examined by X-ray diffraction using (Philips PW) X-ray diffractometer system. Morphological study was carried out by scanning electron microscopy (S-4160 HITACHI) which is used to inspect the size and topographies of nano powders under various core materials of specimens at high magnification. The optical absorbance spectra of the samples within the wavelength ranging from (190 - 1100 nm) at room temperature were measured using UV-Visible (SP – 8001 spectrophotometer. Gas sensor characterizations of core/shell nanostructures have been done as H_2S sensor. To characterize and compare sensor performance, a set of parameters should be defined for each sensor, such as sensor response. The sensor response in percentage, S, is defined as the ratio of resistance change by introducing target gas in the air [23].

$$\boldsymbol{S = \left(\frac{R_{gas} - R_{air}}{R_{air}}\right) \times 100}$$

where, Rgas and Rair are the resistance values of the sensor during gas exposure and air, respectively. Also, response and recovery times are two main characteristic parameters for different target gases. Response time is time constant, which sensor needs to change to 90% of its original value. Similarly, the recovery time is defined as the time required to recover to within 10% of the original baseline when the flow of reducing or oxidizing gas is removed.

3. Results & discussion

3.1 XRD analysis

Figure-1(a-c) show the XRD patterns of Ag/NiO, Au/NiO, Cu/NiO core-shell respectively. The peaks in XRD patterns refer to both core metal Ag, Au, Cu and shell metal oxide NiO as shown in Tables-1,- 2,-3, and Figures-1(a, b, c). The crystallographic plane for NiO that its peak at 2θ around 38° was observed for all samples and assigned to (111) of simple cubic NiO. Also the broadening of xrd peaks points to nanosize of the prepared core-shell.

The average crystallite size (D) of films can be calculated by Scherer formula for the preferred plane (111) for NiO to be 2.3, 2.6, 3.4 nm for Cu/NiO, Ag/NiO, Au/NiO respectively. Therefore, additional SEM measurements were used to analyze the grain size and surface morphology of the samples.

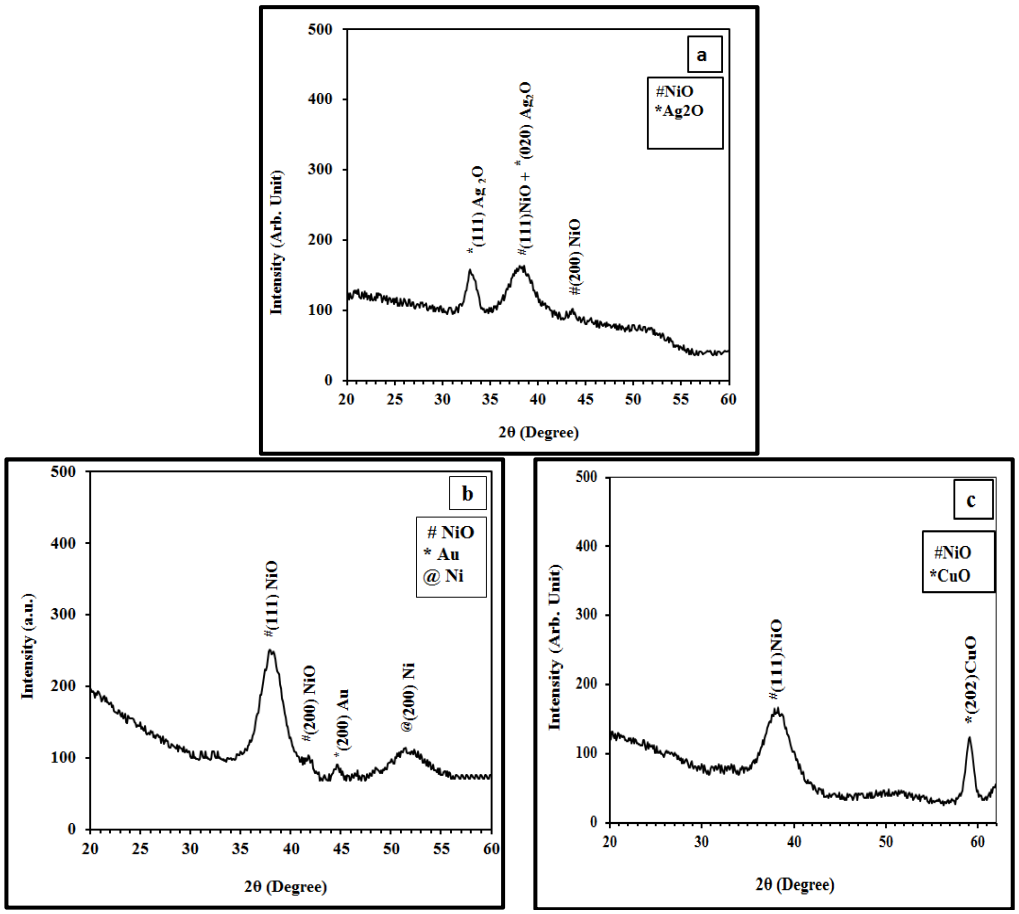

Figure 1- XRD patterns of a) Ag/NiO core-shell; b) Au/NiO core-shell; c) Cu/NiO core-shell powders

Table 1- Structure parameters of Ag/NiO

2θ (Deg.)	FWHM (Deg.)	d_{hkl} Exp.(Å)	Crystallite size (nm)	hkl	d_{hkl} Std.(Å)	Phase	Card No.
32.9996	1.1834	2.7122	7.0	(111)	2.7239	Ag_2O	96-101-0487
38.2185	3.2466	2.3530	2.6	(111)	2.3520	NiO	96-101-0382
				(020)	2.3590	Ag_2O	96-101-0487
43.6194	0.9000	2.0733	9.5	(200)	2.0850	NiO	96-101-0382

Table 2- Structure parameters of Au/NiO

2θ (Deg.)	FWHM (Deg.)	d_{hkl} Exp.(Å)	Crystallite size (nm)	hkl	d_{hkl} Std.(Å)	Phase	Card No.
38.0847	2.5788	2.3609	3.3	(111)	2.3520	NiO	96-101-0382
44.6120	0.6320	2.0295	13.6	(200)	2.0455	Au	96-901-3037
51.7277	4.0971	1.7658	2.2	(200)	1.7935	Ni	96-901-3032

Table 3-Structure parameters of Cu/NiO

2θ (Deg.)	FWHM (Deg.)	d_{hkl} Exp.(Å)	Crystallite size (nm)	hkl	d_{hkl} Std.(Å)	Phase	Card No.
38.2318	3.5805	2.3522	2.3	(111)	2.3520	NiO	96-101-0382
59.0831	0.9705	1.5623	9.4	(202)	1.5724	CuO	96-900-8962
62.2294	1.5171	1.4907	6.1	(-113)	1.4986	CuO	96-900-8962

3.2 SEM analysis

Figures-2, 3, 4, 5 show the SEM images of pure NiO and core-shell powders that prove the nano size of prepared samples. It can be seen that the core-shell samples had a smaller grain size than pure NiO and possessed more porosity especially for Au/NiO core-shell. As a result of smaller grain size and higher porosity, the gas sensing property of the film could change significantly as it will be seen in

the gas sensing results. The grain size was decreased by making core shell structure because of the small size of the core nanoparticles (Ag, Au, Cu) so the NiO is forced to be grown on the nanoparticles of the core so it can be seen that the grain size can be tuned by selecting an appropriate fabricating method and samples which had smaller grains were ideal for gas sensor applications. The SEM images show the surface topography of the powders whereas the XRD patterns show the bulk properties [24].

The surface to volume ratio (S/V) and the degree of porosity are two important parameters, which play important roles in the gas permeability of H_2S in nanomaterials. The high S/V ratio could be obtained by simultaneously decreasing the size of the grains and incorporation more porosity into the structure [25,26].

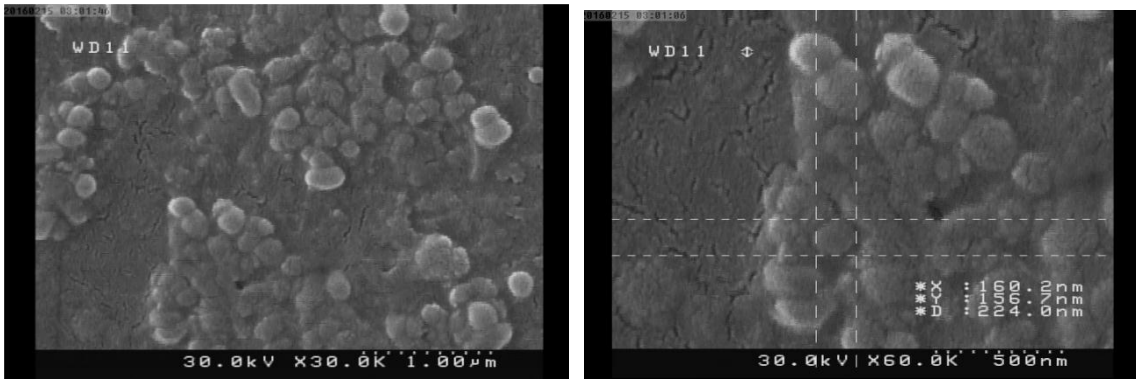

Figure 2- The SEM images of NiO nanoparticle

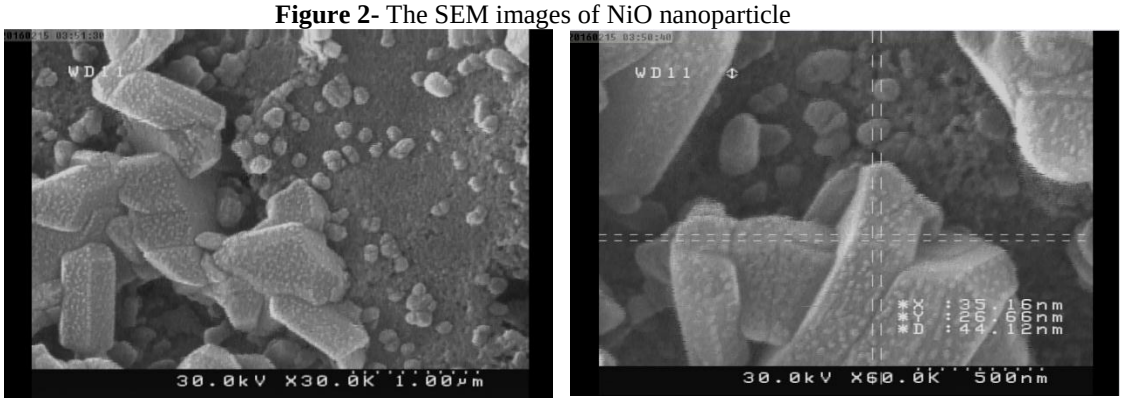

Figure 3- The SEM images of Au/NiO core-shell

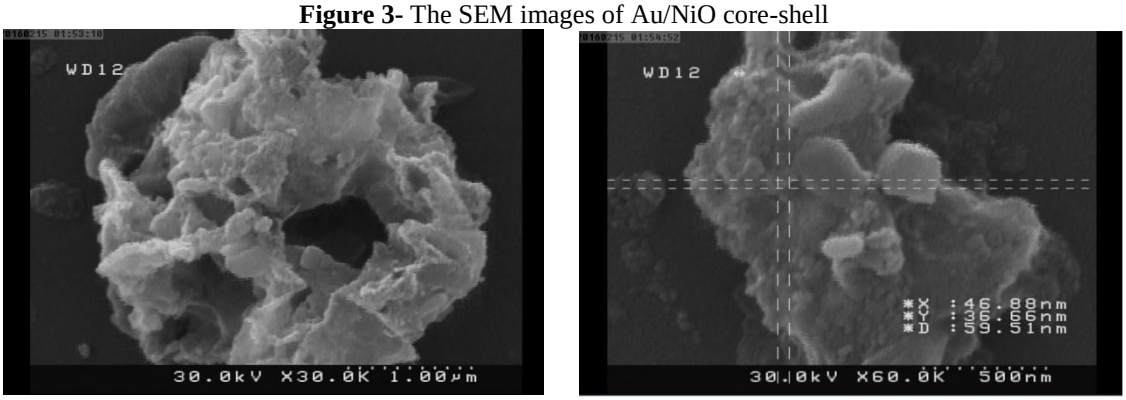

Figure 4- The SEM images of Ag/NiO core-shell

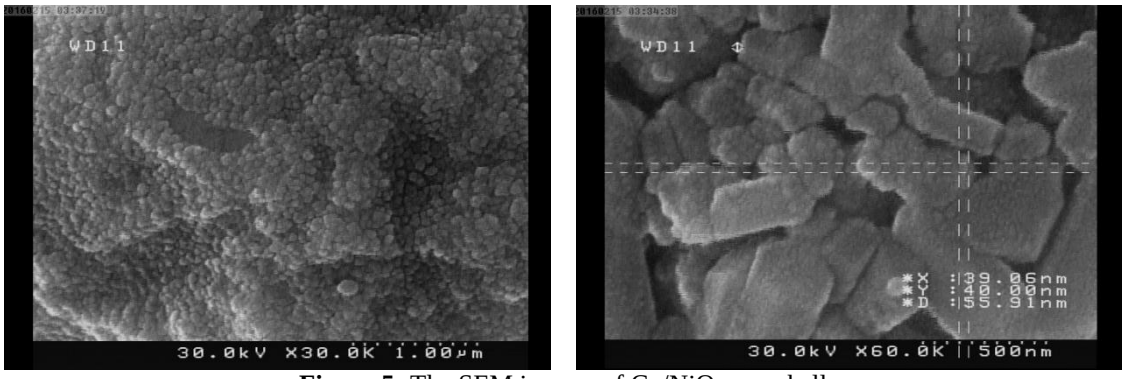

Figure 5- The SEM images of Cu/NiO core-shell

3.3 Optical Properties

Figure-6 shows the optical transmittance spectra of the core-shell films coated on the glass substrates. The core-shell sample exhibited transmittance larger than 60% in the visible and near IR range, while the pure NiO exhibits very low transmittance smaller than 10%. The optical gap of the films was calculated in Table-4 which shows that energy gap increases with core-shell samples and this result is in agreement with SEM results.

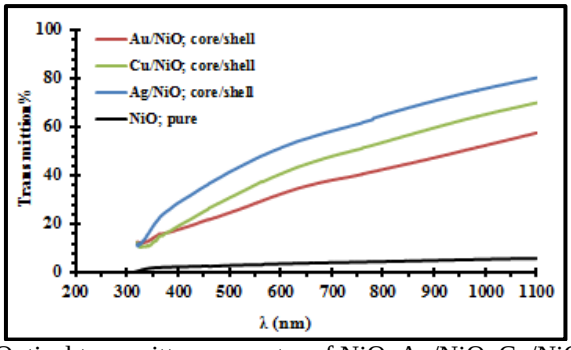

Figure 6- Optical transmittance spectra of NiO, Au/NiO, Cu/NiO, Ag/NiO.

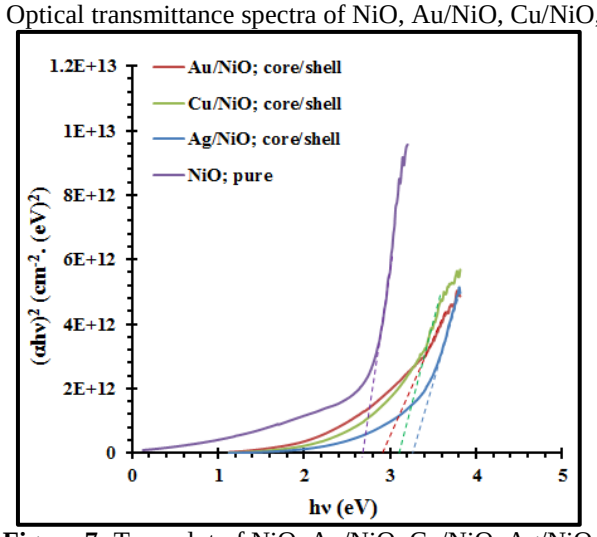

Figure 7- Tauc plot of NiO, Au/NiO, Cu/NiO, Ag/NiO

Table 4- Values of energy gap

Sample	NiO	Au/NiO	Cu/NiO	Ag/NiO
E_g (eV)	2.7	2.9	3.1	3.3

3.4 Gas sensing results

The gas sensing property of the sensor is measured by collecting a change in resistance over two sensing electrodes under H_2S gas. The change in the sensor resistance is attributed to ion adsorption of gas molecules, surface reaction of target gas with adsorbed oxygen on the surface of metal oxide [27]. Adsorbed ions are responsible for a change in conductivity. The negative charged ions are responsible for absorbing electrons and upward band bending around the edge of the grain. By absorbing oxygen

molecules on the surface of metal oxide, they extract electrons from the conduction band E_c and electrons trap at the surface in form of ions. This mechanism causes a band bending and the electron depleted region near the surface of each grain [28]. During the adsorption process at elevated temperatures, different oxygen species are formed on the surface of NiO as O_2^- and O^-[29].

The sensing mechanism of metal oxide gas sensors can be explained by the adsorption of oxygen on the surface of metal oxide grains and its reaction with H_2S gas molecules. By introducing H_2S gas molecules, the electrical conductivity of film changes due to the surface reactions at the grains. The reaction summary can be expressed by:

- H_2S Sensing Electrode Reaction: $\boldsymbol{H_2S + 4H_2O \longrightarrow H_2SO_4 + 8H^+ + 8e^-}$
- H_2S Counter Electrode Reaction: $\boldsymbol{8H^+ + 2O_2 \longrightarrow 4H_2O}$

Figures-8(a, b, c) show gas sensing behavior for NiO where there is weak response.

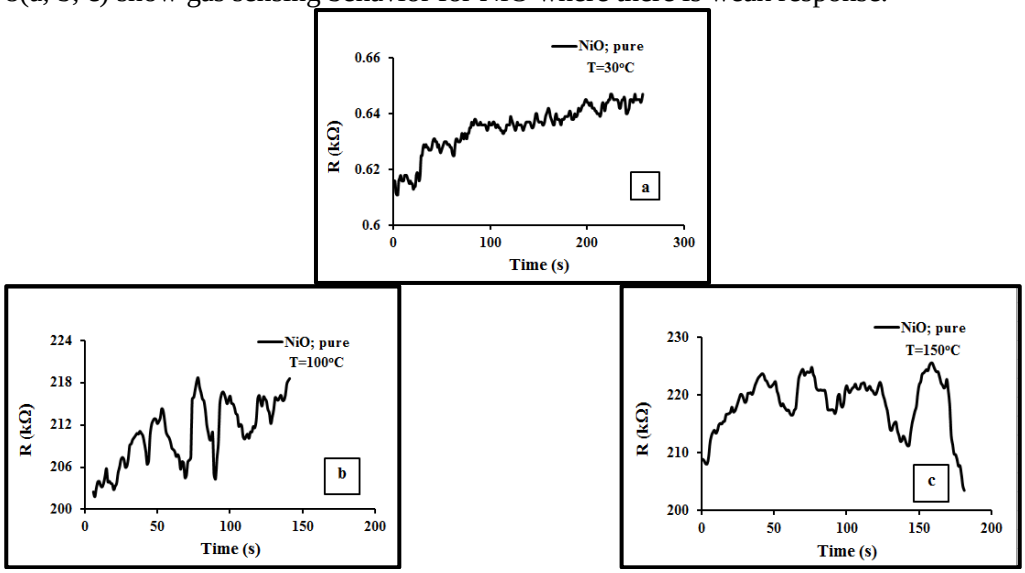

Figure 8-Weak sensing response of NiO to H_2S gas

The gas sensing property of the film was improved significantly due to the catalyst effect of Au, Ag, Cu nanoparticles in the structure of metal oxide. These new core-shell structures increased sensing property of nickel oxide by decreasing the energy needed for splitting H_2 or O_2 molecules on the surface of metal oxide.

The key advantages are: 1) power consumption is minimal because the actual sensing chemical reaction creates the base sensing signal (i.e. each molecule of H_2S produces 8 electrons of signal) and 2) the working electrode reaction regenerates the exact amount of water (H_2O) which was used on the sensing electrode to react with the target gas H_2S, it refills itself.

When oxygen species are adsorbed on the surface of NiO grains, they act as a surface acceptor and force electrons to be removed from the lattice. Further reaction of these adsorbed oxygen ions with reducing gas causes a decrease in band bending and changes the conductivity of grain.

The H^+ react with adsorbed oxygen ions and form water vapor, and as a result of this reaction, electron transfer back to the film according to the reaction [30]. Therefore, the transfer of electrons to the conduction band of semiconductor changes the conductivity of the film. For p-type semiconductor, the transfer of electrons to the conduction band makes the semiconductor less p-type, and the film resistance increases. On the other hand, for n-type semiconductor material, the resistance decreases with increasing the number of electrons in the film. As described in the previous section, metal oxide gas sensors show a change in a resistance in contact with H_2S target gas at different operating temperatures. To improve sensor performance, noble metals such as Au, Ag and Cu are used as active catalysts. These noble metals enhance the reaction between target gas (especially reduced gases) and oxygen molecules [31]. Spill over is a term, which is used to describe the diffusion of adsorbed species from an active site (noble metal) to a non-active site. These sites enhance the speed of molecule dissociation [32]. It has been reported that noble atoms decrease the energy needed to split H_2 or O_2 atoms on the surface of metal oxide thin films [33]. Repeatability determines suitability of the gas sensor for practical applications [34, 35].

Figure-9 (a-i) show the repeatability of the NiO sample for H_2S gas at different operating temperatures. It was found that the response and recovery times were almost constant for each cycle.

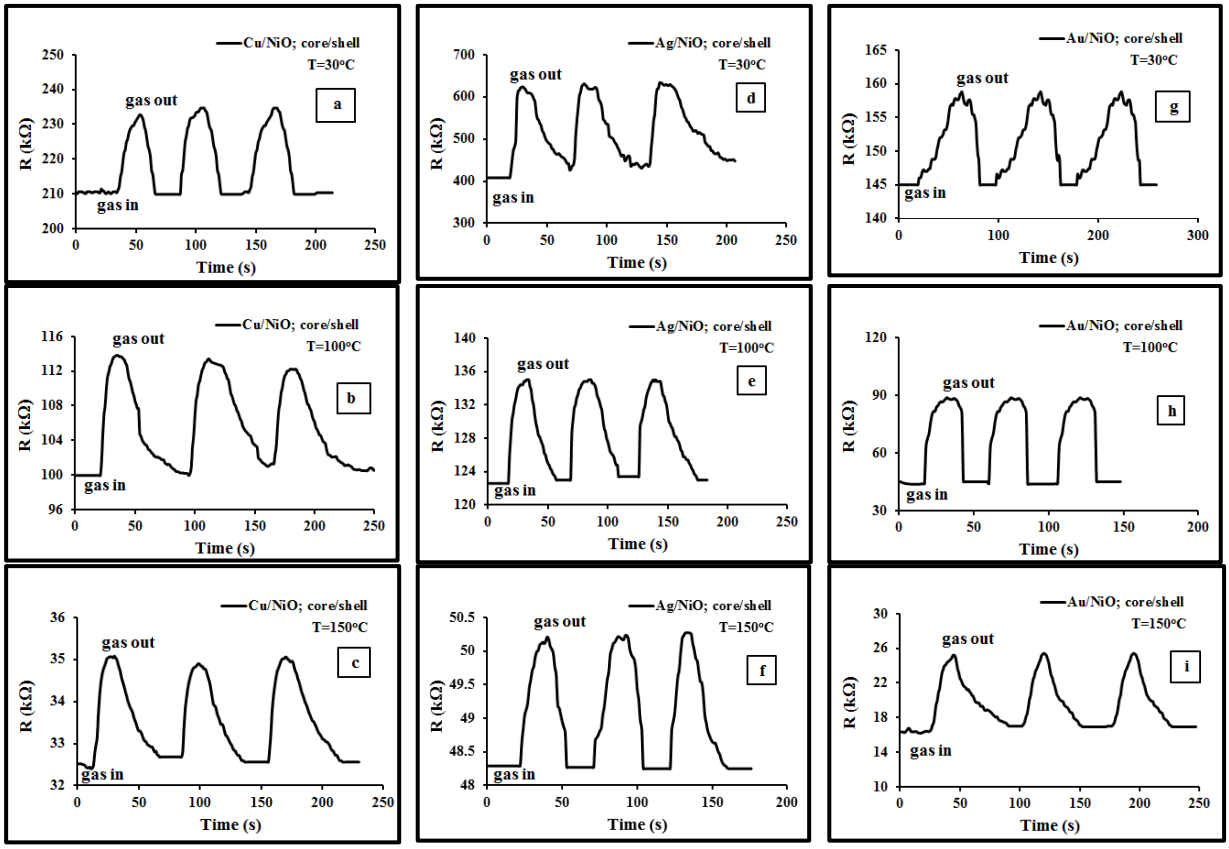

Figure 9- Repeatability of the core-shell structures for H_2S gas at different operating temperatures; (a-c) for Cu/NiO, (d-f) for Ag/NiO, (g-i) for Au/NiO

Table 5- Sensitivity, response and recovery times of core-shell structures at different operating temperatures

core/shell	Ag/NiO			Cu/NiO			Au/NiO		
Temperature °C	RT	100	150	RT	100	150	RT	100	150
Sensitivity %	53	11	58	12	15	9	12	88	54
Response Time (s)	5	7	11	12	6	7	32	7	11
Recovery Time (s)	22	17	8	8	28	23	11	2	22

From Figure-9h and the results of Table-5, we have highest sensitivity with Au/NiO core-shell at working temperature 100°C, also very fast recovery time that means the sensor need ~2s to return to its initial value and be ready to the following signal for entering gas. This result is illustrated in Figure-10.

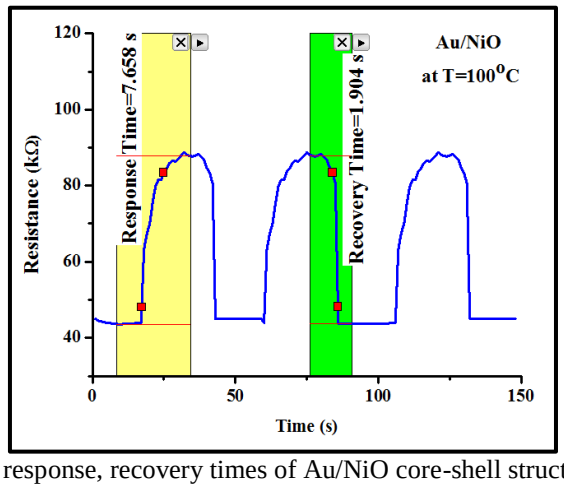

Figure 10- Repeatability, response, recovery times of Au/NiO core-shell structures for H_2S gas at 100°C working temperature

4. Conclusion

This investigation reports on the growth of noble metal/NiO core-shell nanostructures and the fabrication of the H_2S gas sensors based on these core-shell nanostructures. These new structures demonstrate good sensitivity and stable repeatability with time. The H_2S gas detection of the (Ag, Au, Cu) /NiO core-shell sensors present its best response (<32 s) and recovery period (<28 s) with greater repeatability at low operating temperature. The results indicate that the developed noble metal/NiO core-shell nanowires based sensors are highly promising for industrial applications.

References

1. Wetchakun, K. **2011**. Semiconducting metal oxides as sensors for environmentally hazardous gases. *Sensors and Actuators B: Chemical*, 160(1), pp:580-591.
2. Hübert , T. **2011**.Hydrogen sensors – A review. *Sensors and Actuators B:Chemical*, 157(2), pp:329-352.
3. Nenov, T.G. and Yordanov, S.P.**1996**. *Ceramic Sensors-Technology and Applications*; Technomic Publishing: Lancaster, PA, USA.
4. Meixner, H. and Lampe, U. **1996**. Metal oxide sensors. *Sens. Actuat. B:Chem.*, 33, pp:198–202.
5. Moseley, P.T. **1997**. Solid state gas sensors. *Meas. Sci. Technol.*, 8, pp:223–237.
6. Korotcenkov, G. and Cho, B.K. **2009**. Thin film SnO2-based gas sensors: Film thickness influence. *Sensors and Actuators B: Chemical*, 142(1), pp: 321-330.
7. Korotcenkov, G. **2008**. The role of morphology and crystallographic structure of metal oxides in response of conductometric-type gas sensors. *Materials Science and Engineering Reports*, 61(1-6), pp:1-39.
8. Lu, Y.M., Hwang, W.S. and Yang, J.S. **2002.** Effects of substrate temperature on the resistivity of non-stoichiometric sputtered NiO films. *Surface and Coatings Technology*, 155, pp:231-235.
9. Lathamaragatham, A. **2015**. Characterization of Nickel Oxide Nanoparticles Synthesized Via Solution-Phase Precursor Route, International Conference on Systems, Science, Control, Communication, Engineering and Technology ICSSCCE, pp: 216-220.
10. Ahmed, S. S., Hassan, E K. and Mohamed, G. H.**2014**. Investigation of Optical Properties of $NiO_{0.99}Cu_{0.01}$ Thin Film by Thermal Evaporation Technique, *International Journal of Advanced Research*, 2(2), pp:633-638.
11. Nandapure, B. I., Kondawar, S. B. and Nandapure, A. I.**2012**. Magnetic Properties of Nanostructured Cobalt and Nickel Oxide Reinforced Polyaniline Composites, International Conference on Benchmarks in Engineering Science and Technology ICBEST Proceedings.
12. Chai, P.V., Ba-Abbad, M. M., Teow, Y. H. and Mohammad, A.W. **2015**. Low Temperature Condition For NiO Nanoparticles Preparation Via Sol-Gel Method, Proceedings of 25th The IIER Int. Conference, Kuala Lumpur, Malaysia, 2nd May.
13. Imtiaz, A. and Rafique, U. **2011**. Synthesis of Metal Oxides and its Application as Adsorbent for the Treatment of Wastewater Effluents, *Int. Journal of Chemical and Environmental Engineering*, 2(6).
14. Needham, S.A., Wang, G.X. and Liu, H.K. **2006**. Synthesis of NiO nanotubes for use as negative electrodes in lithium ion batteries, *Journal of Power Sources*, 159 (2006), pp:254–257.
15. Nwanya, A. C., Ezema, F. I. and Ejikeme, P. M. **2011**. Dyed sensitized solar cells: A technically and economically alternative concept to p-n junction photovoltaic devices, *Int. Journal of the Physical Sciences*, 6 (22), pp:5190-5201.
16. Mohammadyani, D., Hosseini, S.A. and Sadrnezhaad, S.K. **2012**. Characterization of Nickel Oxide Nanoparticles Synthesized Via Rapid Microwave-Assisted Route, *Int. Journal of Modern Physics*, 5, pp:270–276.
17. Heo, Y. W., Varadarajan, V., Kaufman, M., Kim, K., Norton, D.P., Ren, F. and Fleming P. H. **2002**.Site specific growth of ZnO nanorods using catalysis-driven molecular-beam epitaxy. *Appl. Phys. Lett.*, 81, pp:3046–3048.
18. Hsu, C.L., Chang, S.J., Hung, H.C., Tseng, Y.K., Lin, Y.R., Huang, C.J. and Chen, I.C. **2005**. Well aligned vertically Al-doped ZnO nanowires synthesized on ZnO:Ga/glass templates. *J. Electrochem. Soc.*, 152, pp:G378–G381.
19. Hsu, C.L., Chang, S.J., Lin, Y.R., Tseng, Y.K., Tsai, S.Y. and Chen, I.C. **2005**. Vertically well aligned Pdoped ZnO nanowires synthesized on ZnO:Ga/glass templates. *Chem. Comm.*, 28, pp:3571–3573.

20. Bochenkov, V.E. and Sergeev, G.B. **2010**. *Metal Oxide Nanostructures and Their Applications*.3, American scientific publishers.

21. Hsu, C.L., Lin, Y.R., Chang, S.J., Tseng, Y.K., Tsai, S.Y. and Chen, I.C. **2005**.Vertical ZnGa2O4/ZnO nanorods core shell grown on ZnO/glass template by reactive evaporation. *Chem. Phys. Lett.*, 411, pp:221–224.

22. Hsu, C.L., Lin, Y.R., Chang, S.J., Lu, T.H., Lin, T.S., Tsai, S.Y. and Chen, I.C. **2006**. Influence of the formation of the second phase in ZnO/Ga nanowire systems. *J. Electrochem. Soc.*, 153, pp:G333–G336.

23. Soleimanpour, A. M., Hou, Y. and Jayatissa, A. H. **2011**. The effect of UV irradiation on nanocrysatlline zinc oxide thin films related to gas sensing characteristics. *Applied Surface Science*, 257(12), pp:5398-5402.

24. Korotcenkov, G. **2008**. The role of morphology and crystallographic structure of metal oxides in response of conductometric-type gas sensors. *Materials Science and Engineering Reports*, 61(1-6), pp:1-39.

25. Wang, C. **2010**. Metal oxide gas sensors: sensitivity and influencing factors. *Sensors*, 10(3), pp:2088-106.

26. Dinesh, K.A. and Shiv, K.G. **2007**. *Science and Technology of Chemiresistor Gas Sensors*, p:380.

27. Kohl, D. **1989**. Surface processes in the detection of reducing gases with SnO2-based devices. *Sensors and Actuators*, 18(1), pp:71-113.

28. Yongki, M. **2003**. *Properties and Sensor Performance of Zinc Oxide Thin Films* in *Department of Materials Science and Engineering*, Massachusetts Institute of Technology: USA. p:152.

29. Shoou, J.C. **2010**. High sensitivity of a ZnO nanowire-based ammonia gas sensor with Pt nano-particles. *Nano Communication Networks*, 1(4), pp:283-288.

30. Cappus, D. **1995**. Polar surfaces of oxides: reactivity and reconstruction, *Surface Science*, 337, pp:268-277.

31. Bochenkov, V.E. and Sergeev, G.B. **2010**. *Metal Oxide Nanostructures and Their Applications*.3. American scientific publishers.

32. Korotcenkov, G. **2010**. *Chemical Sensors Fundamentals of Sensing Materials Volume 1: General Approaches*.1, Taiwan: Momentum Press. p:388.

33. Bowker, M. **2000**. In consideration of precursor states, spillover and Boudart's 'collection zone' and of their role in catalytic processes. *J. of Molecular Catalysis A: Chemical*, 163(1–2), pp:221-232.

34. Steinebach, H. **2010**. H_2 gas sensor performance of NiO at high temperatures in gas mixtures. *Sensors and Actuators B: Chemical*, 151(1), pp:162-168.

35. Meixner, H. and Lampe, U. **1996**. Metal oxide sensors. *Sensors and Actuators B:Chemical*, 33(1–3), pp:198-202.